Fast Computation of the Acoustic Field for Ultrasound Elements

H. Emre Güven, *Student Member, IEEE*, Eric L. Miller, *Senior Member, IEEE*, and Robin O. Cleveland

***Abstract*—A fast method for computing the acoustic field of ultrasound transducers is presented with application to rectangular elements that are cylindrically focused. No closed-form solutions exist for this case but several numerical techniques have been described in the ultrasound imaging literature. Our motivation is the rapid calculation of imaging kernels for physics-based diagnostic imaging for which current methods are too computationally intensive. Here, the surface integral defining the acoustic field from a baffled piston is converted to a 3-D spatial convolution of the element surface and the Green's function. A 3-D version of the overlap-save method from digital signal processing is employed to obtain a fast computational algorithm based on spatial Fourier transforms. Further efficiency is gained by using a separable approximation to the Green's function through singular value decomposition and increasing the effective sampling rate by polyphase filtering. The tradeoff between accuracy and spatial sampling rate is explored to determine appropriate parameters for a specific transducer. Comparisons with standard tools such as Field II are presented, where nearly 2 orders of magnitude improvement in computation speed is observed for similar accuracy.**

I. Introduction

Traditional diagnostic ultrasound B-scan images are formed using delay-and-sum beamforming methods based on data collected from transducers comprised of 1-D arrays of transmitter-receiver elements [1]. Although highly useful for a variety of tasks, these images are essentially qualitative in that they do not provide a quantitatively accurate representation of the physical characteristics of the tissue such as sound speed, density, and attenuation [2]. The ability to recover quantitative properties is desirable in a range of application areas, which has motivated the development of ultrasound tomographic image formation systems and algorithms [3]–[9].

A key component of diffraction tomography is the accurate computation of the acoustic field. This is certainly the case for inverse scattering-type methods based on the full Lippman-Schwinger integral equation [10] as well as linearized schemes using the Born or Rytov approximations [9]. For these methods, one requires the evaluation of the field over a large number of spatial locations, thus a key practical requirement for the implementation of diffraction tomography is the efficient computation of the transducer field.

One approach to calculating the acoustic field is to determine the spatial impulse response (SIR) which gives the spatial response to a delta function excitation of the transducer. The mathematical expression for the SIR can be stated simply in terms of the integral of the Green's function over the element surface, and closed-form expressions for the SIR exist for a limited class of transducers [1, Ch. 7], [11]–[13], (flat pistons, flat sectors, flat polygons, and spherically focused bowls or segments thereof). Unfortunately, no exact expression exists for the SIR of cylindrical transducers of the type used in ultrasonic arrays, although approximate methods based on decomposing the element surface into thin strips have been developed [14] and employed in the widely used Field II program [15]. Additionally, exact expressions for the SIR are not available for lossy media and one either needs to employ alternative discretization approaches to incorporate loss directly [16] or approximate the effect of loss through a material transfer function [1, Sec. 4.2].

If the SIR is cast in the frequency domain then lossy, dispersive media can be accommodated through an appropriate choice of the wavenumber. In this manuscript we refer to the frequency domain equivalent of the SIR as the spatial transfer function (STF). The angular spectrum technique [17, Sec. 3.10] is a method of computing the STF but it is computationally expensive and requires migrating the source condition to a plane for curved transducers [18]–[20]. The Fresnel approximation provides a very efficient means of computing of the STF. Traditionally, it can achieve accurate results only in regions close to focal axis [1, Sec. 6.2] however recently an alternative expansion has extended the region of validity [21]. A semi-analytic frequency domain approach considered in [18] yielded a numerical scheme that was highly accurate; however the computational time was still an issue. Moreover, the work in [18] was specifically tailored to a cylindrically concave transducer and not obviously extendable to general curved surfaces.

In the present paper, we describe a new approach to the calculation of the STF. In contrast to the largely analytical approach of [18], the current method is based on computational techniques from the digital signal processing (DSP) community. Specifically, we take advantage of the fact that for the imaging problems and processing schemes of interest in this work the transducer fields are required

Manuscript received September 4, 2008; accepted April 30, 2009. This work was supported in part by CenSSIS, the Center for Subsurface Sensing and Imaging Systems, under the Engineering Research Centers Program of the National Science Foundation (Award Number EEC-9986821) and by the NIH through R21 CA 123523.

H. E. Güven is with the Department of Electrical and Computer Engineering, Northeastern University, Boston, MA 02115 (e-mail: h.emreguven@gmail.com).

E. L. Miller is with the Department of Electrical and Computer Engineering, Tufts University, Medford, MA 02155.

R. O. Cleveland is with the Department of Mechanical Engineering, Boston University, Boston, MA 02215.

Digital Object Identifier 10.1109/TUFFC.2009.1266

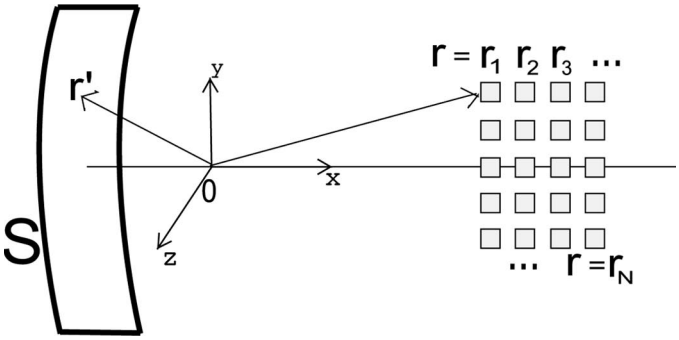

Fig. 1. Variables regarding the spatial transfer function. One could evaluate (1) numerically; however, this approach is inefficient because it does not take into account the shift invariant structure of the kernel.

over a dense set of points located on a regular grid in the region of interest. As such, a highly efficient method based on the fast Fourier transform (FFT) is used to compute the STF in a frequency-dependent attenuating medium. Although the FFT has been employed for accelerating computations similarly in the context of k-space methods [22], in its present use, the overlap-save method from DSP [23], [24], the singular value decomposition (SVD) [25], [26], and polyphase filtering [27] further accelerate the required calculations.

In what follows, Section II provides the background of the physics-based imaging problem and the role of the STF. The proposed approach for computing the STF is presented in Section III, followed by comparisons to previous methods in literature (Section IV) through the example of cylindrically focused transducers. Section V concludes the paper.

II. Background

In this section, a brief review of the problem and the relevant mathematical tools is provided. The STF for the transducer mounted in a rigid baffle can be obtained from the Rayleigh integral (see, for example, [28, Eq. 5-2.6])

$$h(\mathbf{r}) = \int_{\mathbf{r}'\in S} g(\mathbf{r}-\mathbf{r}')\, d\mathbf{r}', \tag{1}$$

where S represents the element surface, $\mathbf{r} = [xyz]^T$ is the coordinate vector, and $g(\mathbf{r}-\mathbf{r}')$ is the Green's function for a point source in a rigid baffle given by

$$g(\mathbf{r}-\mathbf{r}') = \frac{e^{-jk|\mathbf{r}-\mathbf{r}'|}}{2\pi|\mathbf{r}-\mathbf{r}'|}. \tag{2}$$

Here $k = \omega/(c_b(\omega)) - j\alpha_b(\omega)$ is the wavenumber, $\alpha_b(\omega)$ is the attenuation coefficient, and $c_b(\omega)$ is the frequency-dependent sound speed of the medium. Fig. 1 illustrates the variables in (1), where the region of interest consists of N discrete points in space.

A. Spatial Transfer Function as a Convolution

Alternatively, one can view (1) as a convolution of the element surface and the Green's function. Starting with the definition of the indicator function $w(\mathbf{r})$ of the element surface S

$$w(\mathbf{r}) = \delta\big(\mathbf{r} - \mathcal{P}_S\mathbf{r}\big), \tag{3}$$

where $\mathcal{P}_S$ is the spatial projection onto S such that $\mathbf{r} - \mathcal{P}_S\mathbf{r} = 0$ only if $\mathbf{r} \in S$, one can express (1) in 3-D space as

$$h(\mathbf{r}) = \int_V w(\mathbf{r}')g(\mathbf{r}-\mathbf{r}')d\mathbf{r}' \tag{4}$$

$$= (g * w)(\mathbf{r}), \tag{5}$$

where * denotes a 3-D spatial convolution. At first glance, replacing a 2-D surface integral with a 3-D convolution would appear to result in higher computational cost, however it enables the use of Fourier transform methods for numerical calculation of the integral. Because spatial convolution is equivalent to multiplication in the spatial frequency domain, the relation transforms to

$$h(\mathbf{r}) = \mathcal{F}^{-1}\big\{\mathcal{F}(g)\cdot\mathcal{F}(w)\big\}(\mathbf{r}), \tag{6}$$

where $\mathcal{F}$ and $\mathcal{F}^{-1}$ represent the forward and inverse Fourier transform operations, such that

$$G(\boldsymbol{\rho}) = \int_{-\infty}^{\infty} g(\mathbf{r})e^{-j2\pi\mathbf{r}\cdot\boldsymbol{\rho}}d\mathbf{r}, \tag{7}$$

$$g(\mathbf{r}) = \int_{-\infty}^{\infty} G(\boldsymbol{\rho})e^{j2\pi\mathbf{r}\cdot\boldsymbol{\rho}}d\boldsymbol{\rho}, \tag{8}$$

where $G = \mathcal{F}(g)$. By employing the fast Fourier transform, it is therefore possible to perform the computation at a reduced complexity compared with direct calculation.

B. Practical Challenges

Whereas the use of fast Fourier method for efficient computation of convolution is commonplace [23], [24], [29], there are several issues associated with the specific nature of the current problem that must be overcome to realize the computational gains. Four such issues are addressed in this manuscript:

1. Technically, fast Fourier transform methods may only be used for the calculation of convolutions involving finite length signals. Whereas $w(\mathbf{r})$ does have such compact support, $g(\mathbf{r})$ is infinite in extent both in space and spatial frequency. However, because h is of interest only over a finite support, it is possible to truncate g. In the case of 1-D signal processing there exist efficient block-processing methods for using the FFT to compute convolutions between signals of radically different lengths [30, Ch. 18]. These methods are adapted for the multidimensional problem of interest in this paper.
2. The support of the transducer, indicated by $w(\mathbf{r})$, is not truly a 3-D function, but rather a 2-D surface

embedded in 3-D. In essence, in the direction normal to the surface of the element, $w(\mathbf{r})$ resembles a delta function, leading to a flat spectrum associated with the corresponding dimension. Even if the spatial Fourier transform of such singular functions can be found for some transducer surfaces such as planar rectangular or circular pistons, for more general transducers such as the cylindrically concave elements of specific interest to us, no such closed-form expressions exist. Thus, care must be taken in the development of a numerical method for computing the spatial Fourier transform of $w(\mathbf{r})$.

3. The surfaces of many common transducers are at least partially separable functions of x, y and z. For example, referring to Fig. 1, the cylindrically concave transducer takes the form $w(x, y, z) = u(x, y)\, v(z)$, where $u(x, y)$ represents a circular arc, and $v(z)$ is a rect function [29] associated with the width of the transducer. For convolution problems where both functions are separable, lower-dimensional Fourier transforms may be applied in parallel with the individual results, then merged to form the full 3-D solution. Although g is not separable in general, we demonstrate here that an accurate decomposition in terms of few separable components can be obtained using the SVD, thereby yielding additional computational savings.
4. The accuracy of the method depends heavily on the spatial sampling rate because of the abrupt spatial characteristics of the transducer elements. Whereas one typically desires on the order of 10 samples of the STF per wavelength, we show that this spatial sampling rate is insufficient for adequately representing the surface of the transducer element. The convolution can be performed at an increased spatial sampling rate only to meet the sampling requirement, then the output can be downsampled; but this approach requires more memory and computation time than is really necessary. To avoid this added cost, we employ polyphase filtering [27] to achieve the same improved accuracy as using higher sampling rate by using a bank of filters to characterize the surface of the element. This approach has the added benefit of offering a parallel implementation of the STF calculation.

III. Technique

In this section, the computational scheme is described in detail. The purpose is to find the 3-D convolution of g and w on a discrete grid. Discretization of the element surface w is subsequently treated in Section III-B. For now, assume that the 3-D convolution is expressed in a discrete setting as

$$h(x, y, z) = \sum_{x', y', z'} w(x - x', y - y', z - z')\, g(x, y, z). \tag{9}$$

Because g is of infinite spatial support, and the support of w is significantly smaller than the region of interest in h; it is computationally efficient to divide g into blocks using the overlap-save method [24], [31]. Thus we focus on processing at the block level for the rest of the paper. For each block, the separability of the element surface is used to reduce the dimension of the convolution. The Green's function g is separated over the same spatial block by means of the SVD. The finite convolutions resulting from each separable component can then be linearly combined. Next, a polyphase structure is used to represent the element surface effectively at a higher sampling rate, while requiring shorter FFT lengths. Further details regarding each operation are provided below. In the examples to follow, a 0.5 mm wide × 13 mm high cylindrical element with a focal distance of 70 mm is considered for the calculation of STF near the focal region, for a frequency of 3.5 MHz. This corresponds to the properties of a single element in a B-K 8665 (B-K Medical, Wilmington, MA) curvilinear array. A sound speed of 1500 m/s and a frequency-dependent loss of 0.5 dB/(cm MHz), i.e., 1.75 dB/cm at 3.5 MHz, are assumed, which are representative of soft tissue.

A. Separable Decomposition

Multidimensional convolution can be implemented via lower-dimensional convolutions when corresponding separable components are available. Assuming $w(x, y, z) = u(x, y) \cdot v(z)$ and $g(x, y, z) = \eta(x, y) \cdot \xi(z)$, one can express the 3-D convolution of g and w as

$$(w * g)(x, y, z) = \{(u * \eta)(x, y)\} \cdot \{(v * \xi)(z)\}. \tag{10}$$

When g is expressed as, or closely approximated by, the sum of P separable components

$$g(x, y, z) = \sum_{p=1}^{P} \sigma_p \eta_p(x, y) \xi_p(z), \tag{11}$$

the identity in (10) can be used to express the convolution of g and w as

$$(w * g)(x, y, z) = \sum_{p=1}^{P} \sigma_p \{(u * \eta_p)(x, y)\}\{(v * \xi_p)(z)\}, \tag{12}$$

which provides computational efficiency because this form requires fewer multiplications per output sample when P is relatively small. For example, for a region of interest of size $N_1 \times N_2 \times N_3$ points, realization of the 3-D convolution would normally be $\mathcal{O}(N_1 N_2 N_3 \log N_1 N_2 N_3)$ without separability, whereas the above decomposition reduces this complexity to $\mathcal{O}\big(P\big[N_1 N_2 \log(N_1 N_2) + N_3 \log N_3\big]\big)$, which is significantly less when P is much smaller than $(N_1 N_2)$ and N_3. Nevertheless, it is worth noting that the major reduction in computational complexity for the problem at hand will be due to the use of the FFT rather than the use of separability. In numerical terms, for the examples of

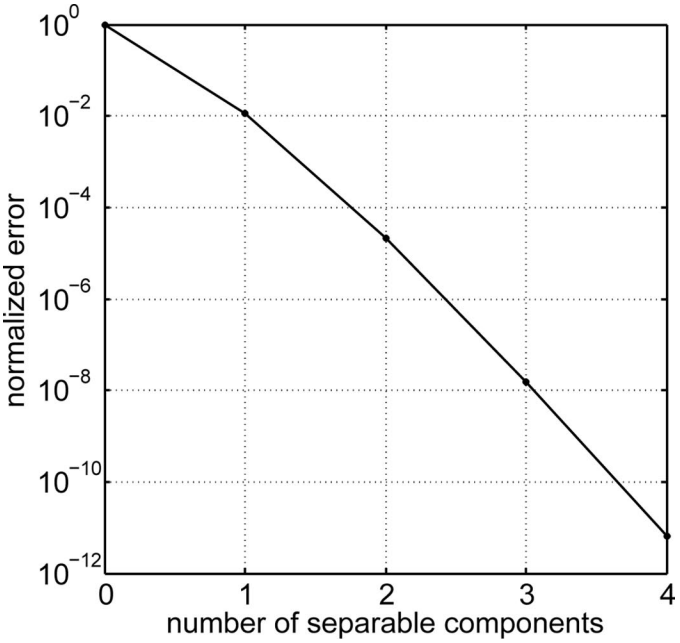

Fig. 2. Error in the approximation of the Green's function.

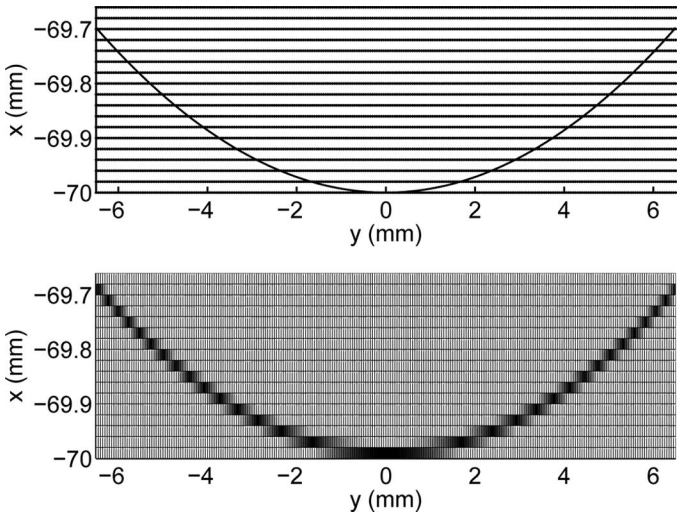

Fig. 3. Top: cross section of element surface (solid) and grid points (·). Bottom: corresponding smoothed function. Consequently, the indicator function for the element surface is available separably as $w(x, y, z) = u(x, y)v(z)$.

this paper, taking advantage of separability in addition to FFT contributed only between 1.2 and 4 times, with the greater contributions occurring for higher effective sampling frequencies.

Although many transducers admit separable expressions, such as the one of interest in this work, the Green's function in 3-space is not exactly separable. Still, as demonstrated below, for the size of the blocks used in the processing scheme (approximately 65 mm^3 or 825 wavelengths cubed), the SVD of the discretized function provides a good approximation of the original function using no more than 2 separable components in each block.

For implementation purposes, a vectorization over (x, y) variables makes it possible to bring the 3-D function into a matrix format, thus allowing the use of matrix SVD. This can be visualized as stacking each 2-D vector corresponding to different $z = z_i$ into a column vector for processing. More explicitly, for each volumetric block, the approximation is given by the first few largest singular vectors $\sum_{p=1}^{P} \sigma_p \eta_p(x, y)\xi_p(z)$, where σ_p is the pth largest singular value associated with vectors $\eta_p(x, y)$ and $\xi_p(z)$, where (x, y) and z denote the discretized support. Fig. 2 shows the normalized approximation error with respect to the number of singular vectors used in the approximation, up to $P = 4$, for a 1000 mm^3 (12 704 wavelength cubed) region starting at the focus at 7 cm axial distance from the transducer. The error is given by $e = 1 - \left(\sum_{i=1}^{P} \sigma_i^2\right) / \left(\sum_{i=1}^{N} \sigma_i^2\right)$, where $\{\sigma_i\}_{i=1}^{N}$ are the corresponding singular values. The figure illustrates the fast decay of the error with respect to the number of linear separable components, even though this volume (1000 mm^3) is much larger than the block volume (65 mm^3) in the examples. In implementation, however, fixing the value of P for all blocks of the overlap-save method may cause varying error levels, so we specify an upper bound on the approximation error, instead. In the examples of Section IV, we specified this tolerance value as 10^{-6}. To avoid excessive computation, we do not compute the full SVD of the matrices arising in our problem. Rather, iterative methods (here, ARPACK as implemented in Matlab, the MathWorks, Natick, MA) are used to compute only a few singular values and vectors. In the examples of Section IV, the number of singular vectors turn out to be $P = 1$ for block (i) that is close to the axis, and $P = 2$ for blocks (ii) and (iii) that are off-axis, respectively.

B. Characterization of the Transducer

The indicator function for an element is defined in (3). As noted earlier, in many cases the element is separable in at least one dimension, so the surface can be represented as $w(x, y, z) = u(x, y) \cdot v(z)$, where $v(z) = \mathrm{rect}(z/z_0)$ for a cylindrically concave transducer with an element width of z_0 along the z-axis.

Ideally u would also be separable but unfortunately, for the transducer elements of interest in this paper as seen in Fig. 3, and indeed for many transducers, $u(x, y)$ is a curve in the (x, y) plane and analytical or numerical computation of its 2-D Fourier transform is a difficult task. The approach taken here is to approximate the infinitesimally thin curve as a finite width function whose transform can in fact be obtained accurately. As is apparent from the examples in the next section, without sacrificing accuracy, this approximation leads to substantial computational advantage in computing the STF relative to alternative methods. Here the function $u(x, y)$ is smoothed using a triangle based linear interpolation of the circular arc onto a rectangular grid using Matlab's griddata function. Fig.

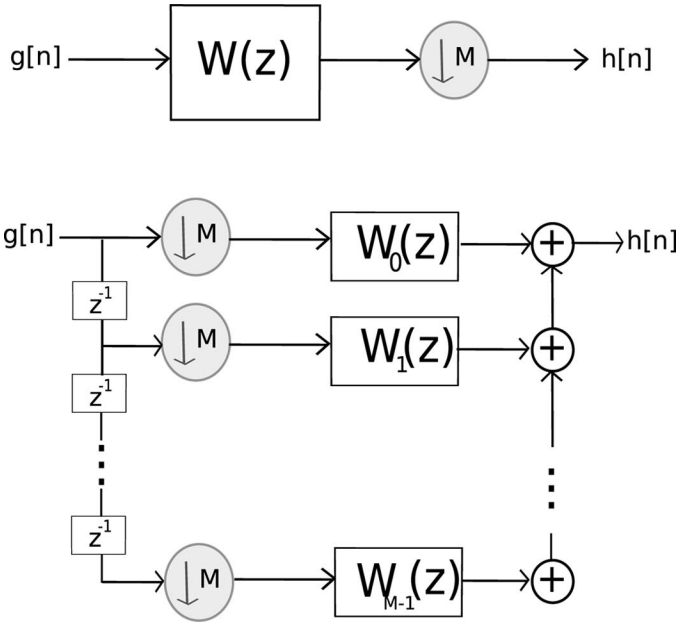

Fig. 4. Equivalent filtering/decimating systems. Top: filtering first followed by decimation. Bottom: signal is downsampled first and then passed through a bank of shorter filters.

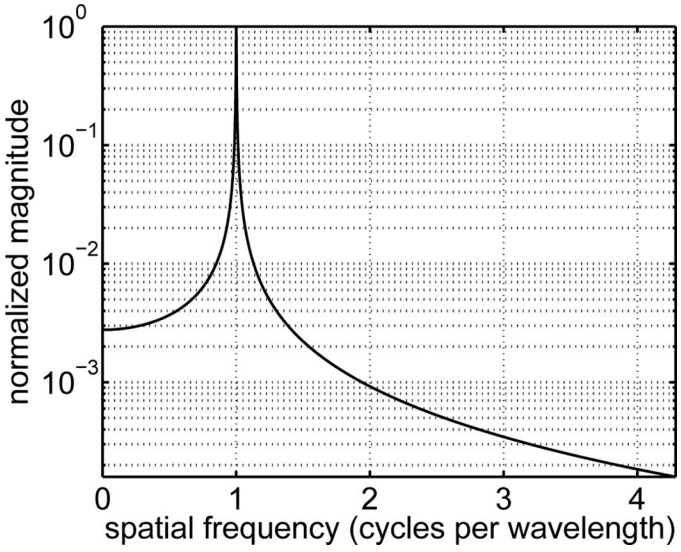

Fig. 5. Magnitude plot of $G(\mathrm{r})$.

3 shows the cross section of the element surface and the corresponding discrete smoothed function.

C. Polyphase Structure

To perform the convolution $(g * w)(\mathbf{r})$ accurately in a discrete setting, the spatial sampling rate needs to be sufficiently high to characterize $g(\mathbf{r})$ and $w(\mathbf{r})$ with minimal aliasing. As we show in the following section, the number of samples required to represent the integral in (4) is much larger than for the representation of the STF needed in practical application. In fact, it is possible to operate at a higher sampling rate initially and then downsample the output, but this method is inefficient because only a small fraction of the computed samples are actually necessary. Polyphase filtering provides a means of achieving the high-rate characterization of the element through a bank of low-rate signals combined by addition. This way, it is possible to avoid the higher computational complexity introduced by the higher sampling rate. Fig. 4 shows 2 equivalent implementations of filtering and decimation. In order for the equivalence of 2 systems to hold, the necessary condition is that

$$w_m[n] = w[Mn + m], \quad m = 0,\ldots,M-1. \tag{13}$$

The required number of multiplications for the former implementation is order $MN\log_2(MN)$, whereas the latter one is $MN\log_2 N$, for the filter $w[n]$ of length N. In addition, the memory requirements of using the lower order is M times less. For a detailed treatment of multirate filter theory the reader is referred to [27].

D. Specification of Parameters

In this section, the implementation of the method is described and the impact of the parameters pertaining to the spatial sampling frequency at the output, the polyphase factor for characterization of the element surface in space, tolerance to error introduced by using a separable approximation to Green's function, and the block size for convolution are investigated.

1) Sampling Rate: To understand the sampling rate requirements caused by Green's function, a good indicator is its spatial Fourier transform, given in polar coordinates by [32]

$$G(\mathbf{r}) = \frac{1/2}{4\pi^2|\mathbf{r}|^2 - k^2}. \tag{14}$$

Fig. 5 shows the magnitude of $G(\mathbf{r})$ up to a spatial frequency of over 4 cycles per wavelength, where the wavenumber is taken to be $14661 - j20.15\ \mathrm{m}^{-1}$ (corresponding to the properties of soft tissue at 3.5 MHz).

As far as arbitrarily shaped elements are concerned, the spatial sampling rate required to characterize the element may differ from that of the Green's function. This is the case for the cylindrically curved elements of interest in this work. The spatial Fourier transform of the arc in Fig. 3 decays very slowly with respect to the Fourier coordinate ρ associated with x. This can be seen from the samples of 2-D Fourier transform magnitude in Fig. 6 associated with the arc in Fig. 3. Because of the relatively flat spectral characteristics of w with respect to g, a higher sampling rate is necessary to compute the convolution than g alone requires, to achieve similar accuracy. Although an exact number depends on the discretization of w, for the linear interpolation scheme used in this paper, it proves sufficient to sample at about 6 times higher rate

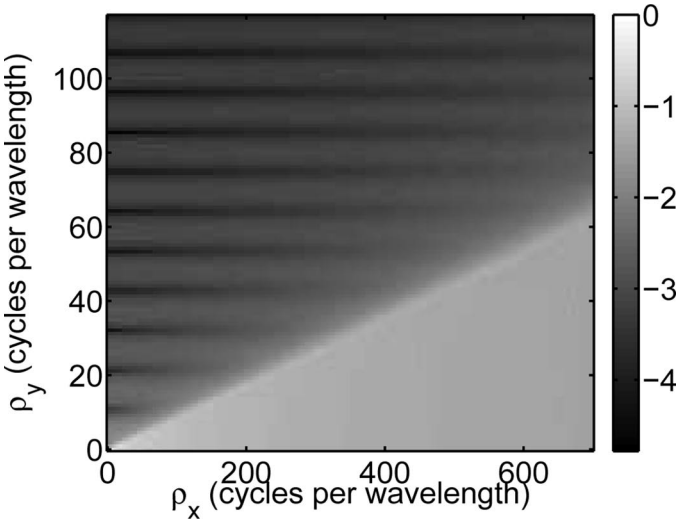

Fig. 6. Log_{10}-magnitude samples of the 2-D spatial Fourier transform of the arc in Fig. 3. ρ_x and ρ_y are the spatial Fourier coordinates associated with x and y, respectively.

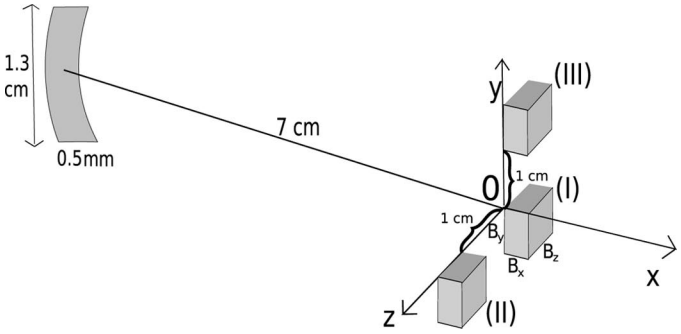

Fig. 7. Comparison setting for the numerical experiments.

than sampling g, i.e., approximately 21 versus 4 samples per wavelength. On the other hand, in practical applications such as model-based imaging, the desired sampling rate for the STF is on the order of 8 to 10 samples per wavelength. Therefore, instead of decimating the output computed at the higher sampling rate, we use an alternative implementation given by the polyphase structure, as the latter is computationally more efficient. The choice of the polyphase factor, M in Fig. 4, which must be chosen so as to address the requirements, is discussed next.

2) Polyphase Factor: As explained previously, for the application of interest there is a discrepancy between desired spatial sampling rate of the STF and that required by the spatial characteristics of the element or the Green's function. The polyphase structure addresses this discrepancy while remaining computationally efficient. The "effective" sampling rate, which determines the accuracy of the computation, is given by $F_e = F_s \cdot M$, where F_s is the desired sampling rate of the STF, and M is the polyphase factor, for each dimension. All the convolution operations are performed at the lower sampling rate F_s as in the bottom implementation of Fig. 4, whereas the achieved accuracy is the same as if operating at F_e as in the top implementation of Fig. 4.

In the multidimensional problem at hand, the number of polyphase components M_x, M_y, M_z need not be identical, so one need not have the same factor of increase in the computational burden for each dimension. The computational complexity of the operation with respect to the polyphase factor is linear for each individual dimension.

3) Block Size: Because the physical problem requires multidimensional convolutions, a version of the overlap-save method generalized to higher dimensions is employed [31]. Similar to the 1-D case, the computation of 3-D Fourier transform requires $O(N\log N)$ multiplications, where N is the total number of samples.

In 1-D filtering applications where the input sequence is much longer than the filter, it is computationally more advantageous to implement the convolution in smaller blocks. Moreover, an optimum value of the block size B can be found by minimization over the required number of multiplications, which is proportional to $\lceil N/(B - L + 1)\rceil B\log_2 B$, where L is the filter length, and N is the desired number of output samples. For large N, the optimal block length B_o is usually in the range $4L \leq B_o < 8L$, and the computational gain is roughly $L/\log_2 B$, growing with the filter length [30, Ch. 18]. Note that the optimal block size may vary for multidimensional problems [33], as a function of the transducer element and the sampling rate in this case. Nevertheless, we do not devote further space to analyze the effect of this optimal block size because we observed little relative improvement over selecting the power of 2 within $[4L, 8L)$ as the block sizes for each dimension. Of further note, the extension of the overlap-save algorithm to multidimensional space can be visualized as overlapping rectangular prisms over the region of interest.

In summary, the parameters considered in this section and how they are determined are as follows.

- *Sampling rate* is effectively determined by the wavenumber.
- *SVD error tolerance* determines the acceptable level of approximation error caused by truncation in the SVD, picked as one part in a million in our example.
- *Polyphase factor* improves accuracy at the cost of computation. Several different factors are considered in the next section.
- *Block size* is determined as a function of the size of the element and the sampling rate so as to yield a low computational cost.

IV. Comparison

We compare our results to previous methods for computing the STF using a scheme similar to that in [18]. Fig. 7 shows the configuration for the field calculation. The source is a 0.5 mm wide, 13 mm high element focused in the elevation plane at 70 mm. The block dimensions were

TABLE I. ERRORS AND COMPUTATION TIMES FOR EVALUATING THE SPATIAL TRANSFER FUNCTION. FOR THE PROPOSED METHOD, THE NUMBERS IN THE LEFT COLUMN GIVE THE CORRESPONDING POLYPHASE FACTORS (M_X, M_Y, M_Z).

	Block (i)		Block (ii)		Block (iii)	
Method	Error (%)	Speed-up factor	Error (%)	Speed-up factor	Error (%)	Speed-up factor
Fresnel	2.25	84.5	8.53	77.3	66.1	82.0
Mast	0.53	62.6	1.30	49.0	5.80	56.9
Field II	3.05	1.2	1.89	1.2	8.24	0.5
SAM	0.30	0.3	0.30	0.4	2.79	0.3
(1,1,1)	1.63	311.2	5.56	260.3	9.89	281.9
(1,2,1)	1.49	209.9	5.53	165.3	7.91	173.1
(2,2,1)	0.53	136.8	5.35	102.9	4.01	112.9
(2,2,2)	0.47	77.8	2.67	60.1	4.01	63.8
(2,3,2)	0.37	53.2	2.65	40.7	2.96	43.1
(3,3,2)	0.29	36.8	2.64	28.6	2.48	30.3

$B_x = 32$, $B_y = 512$, and $B_z = 32$ (at a rate of 20 samples/mm in each direction). The proposed method is compared with the standard Fresnel approximation using plane wave expansion, a recently published Fresnel approximation [21] using the expression for a diffracted spherical wave, Field II [15], and the semi-analytic method (SAM) [18]. Fig. 7 shows the 3 positions of the computed block, one originating from the focus, and the other 2 off-axis.

The implementation of both Fresnel approximations employed the analytical formulae provided in [21] using a Matlab implementation of the complex error function [34]. For Field II, the parameters of the subroutine xdc_focused_array were as follows: no_elements = 1, width = $5 \cdot 10^{-4}$, height = $1.3 \cdot 10^{-2}$, kerf = $1.6667 \cdot 10^{-4}$, Rfocus = $7 \cdot 10^{-2}$, no_sub_x = 1, no_sub_y = 200, and focus = [0, 0, 0.07]. In addition, the excitation signal was specified as $v(t) = \exp\{-(t/T)^4\} \cdot \sin(2\pi f t)$ with $T = 0.2$ μs, $f =$ 3.5 MHz, and $t \in [-0.6, 0.6]$ μs with a sampling interval of 0.002 μs.

The performance criteria for comparing the results h_i of different methods follow those defined in [18], except that complex values of h_i are compared here instead of their magnitudes. The reference solution, h_0, was calculated by a direct numerical approach using Gauss-quadrature integration. A total of 1274 quadrature points (182 along the circular arc in (x, y)-dimensions, times, 7 along the strip in the z-dimension) was employed. The percentage error with respect to h_0 is given by $100||h_i - h_0||_2/||h_0||_2$. The speed-up factor is given by $s_i = t_0/t_i$ where t_0 is the time spent on Gauss-quadrature integration, and t_i is time spent on the corresponding method, including all overhead calculations. Time was determined using the tic and toc functions of Matlab.

Table I indicates the errors and computational speed-up factors for the compared methods for 3 different blocks seen in Fig. 7. The block sizes used in comparison are the same as that used for the FFTs. Figs. 8, 9 and 10 show the real parts of the spatial transfer functions calculated on line segments from the 3 blocks, via the Gauss-quadrature, the proposed method with polyphase factor $(3, 3, 2)$, and Fresnel approximation.

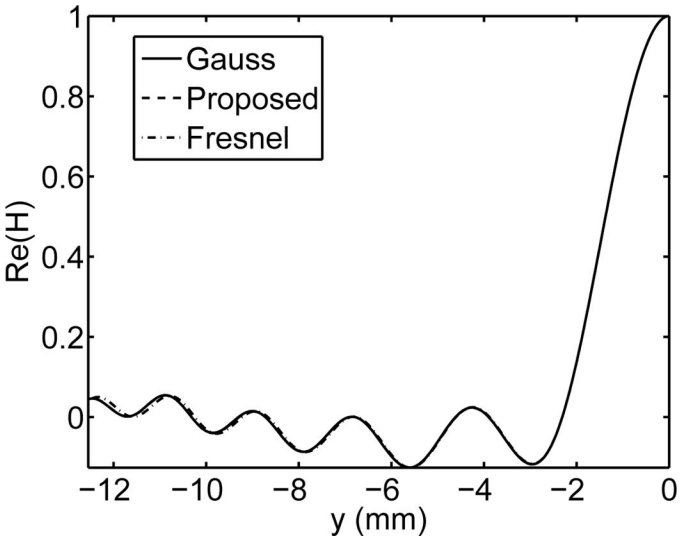

Fig. 8. Real part of the spatial transfer function for $x = 0$, $z = 0$ in block (i). The natural focus of the element is at $y = 0$.

The proposed method provides more than an order of magnitude faster computation with respect to Field II [15] and SAM [18] while maintaining similar levels of error. The modified Fresnel approximation proposed by Mast [21] was comparable in speed and accuracy, although part of its speed may be attributed to the use of an analytical expression which may not exist for more complex geometries. We note that Field II employs a compiled mex file to carry out the calculations, whereas all the other routines were written in native Matlab script. This likely gives Field II an apparent speed advantage which may not be realized if all algorithms were compiled. The 6 different rows for the proposed method in Table I correspond to different polyphase factors. Specifically, the vector (M_x, M_y, M_z) assumes the corresponding values on the first column.

V. DISCUSSION

In this paper, we presented a method for the computation of the spatial transfer function for ultrasound

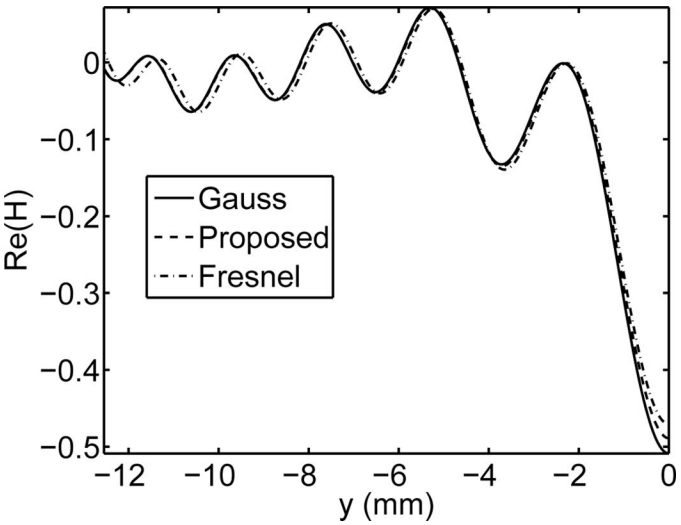

Fig. 9. Real part of the spatial transfer function for $x = 0$, $z = 1$ cm in block (ii).

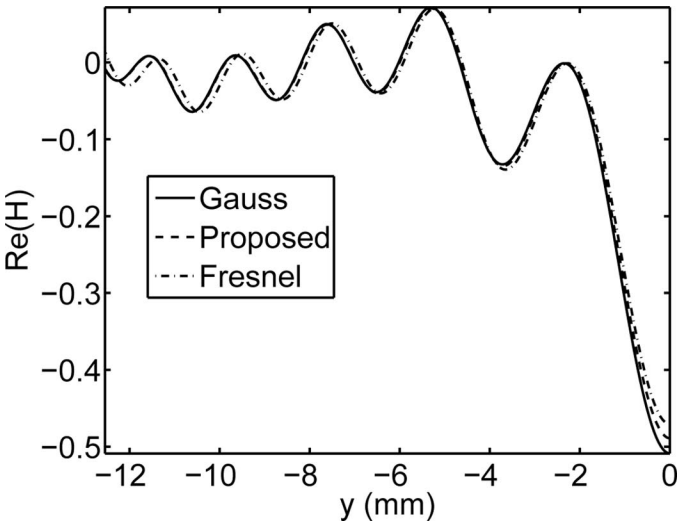

Fig. 10. Real part of the spatial transfer function for $x = 0$, $z = 0$ in block (iii).

transducers, and demonstrated its application to curved rectangular transducers for which no analytic expression exists. Significant computational savings were obtained through the use of FFT to evaluate the spatial transfer function in the spatial frequency domain. Overlap-save, SVD, and polyphase filtering were used to get an accurate method at low computational cost. As a result, speed of computation was improved by more than an order of magnitude relative to Field II and SAM for similar accuracy. Whereas the modified Fresnel approximation by Mast [21] has a closer performance in speed, the method proposed here is applicable even when no analytical solutions are known for the elements.

Using the proposed method, it is possible to reduce the error by increasing the effective spatial sampling frequency, gaining performance at the cost of increased computation time. In contrast to Field II [15] and the frequency-independent approach tailored for cylindrically concave transducer [18], both of which can provide the spatial transfer function at different acoustic frequencies without additional computation time; the proposed method requires separate computation for each frequency of interest. Nevertheless, the reduction in computational complexity with respect to the number of points in space makes the method especially suitable for applications involving many points of interest in space and relatively few frequencies. The parameters of the method are determined according to the wavenumber and desired accuracy. The method is applicable to other curved transducers through discrete characterization of their surfaces.

Appendix
Block Convolution Using FFT

In this appendix, a brief review of the overlap-save method for finite impulse response filtering is presented, in which a relatively long signal is processed with a finite impulse response filter. In this case, the convolution boils down to a finite sum

$$h[n] = \sum_{m=0}^{M-1} w[m] \cdot g[n-m], \tag{15}$$

where $w[m]$ is the finite length filter. Assuming $h[n]$ is of interest for a finite region $n \in [0, N-1]$, a truncated signal $g_t[n]$ is defined to take the same values as $g[n-M]$ for $n \in [0, B-1]$, where $B = M + N$, and identically zero elsewhere. Next, define the B-point discrete Fourier transform $H_t[l]$ such that

$$H_t[l] = \sum_{n=0}^{B-1} \sum_{m=0}^{M-1} w[m] g[n-m] e^{i(2\pi/B)ln} \tag{16}$$

$$= \sum_{m=0}^{M-1} w[m] e^{i(2\pi/B)lm} \sum_{n=0}^{B-1} g[n-m] e^{i(2\pi/B)l(n-m)} \tag{17}$$

$$= W[l] \cdot G_t[l], \tag{18}$$

where we can recognize the last term as the discrete Fourier transform (DFT) of the truncated signal $g_t[n]$. It can be seen by inspection that $\{h[n]\}_{n=0}^{N-1}$ and $\{h_t[n+M]\}_{n=0}^{N-1}$ take exactly the same values, where $h_t[n]$ is the B-point inverse-DFT of $H_t[n]$. In this setting, one can therefore compute $h[n]$ by using the B-point DFT, which can be computed efficiently when B is a power of 2. This way, the convolution of $g[n]$ and the finite length signal $w[n]$ can be computed by shifting the block at every step. This approach is called overlap-save method [24]. Fig. 11 illustrates this scheme.

Acknowledgment

The authors thank B. Karbeyaz for providing the code used for comparison in [18].

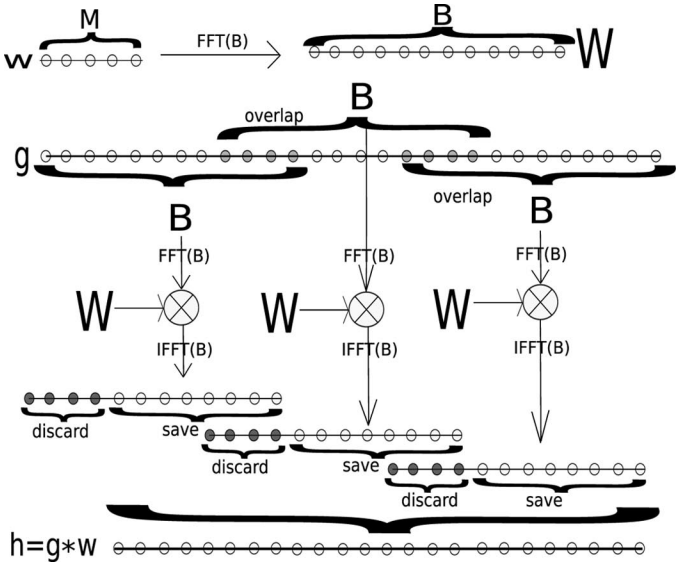

Fig. 11. Illustration of the overlap-save scheme for block convolution using fast Fourier transform.

References

[1] T. Szabo, *Diagnostic Ultrasound Imaging: Inside Out*. Boston, MA: Academic Press, 2004.

[2] J. Mamou, M. L. Oelze, W. D. O'Brien Jr, and J. F. Zachary, "Identifying ultrasonic scattering sites from 3D impedance maps," *J. Acoust. Soc. Am.*, vol. 117, no. 1, pp. 413–423, Jan. 2005.

[3] J. F. Greenleaf, S. K. Kenue, B. Rajagopalan, R. C. Bahn, and S. A. Johnson, "Breast imaging by ultrasonic computed transmission tomography," in *Acoustical Imaging*, A. Metherell, Ed., New York, NY: Plenum Press, 1978.

[4] T. D. Mast, L. Feng, and R. C. Waag, "Time domain ultrasound diffraction tomography," in *Proc. IEEE Ultrasonics Symposium*, vol. 2, Oct. 1999, pp. 1617–1620.

[5] R. R. Leach, Jr., S. G. Azevedo, J. G. Berryman, H. R. Bertete-Aguirre, D. H. Chambers, J. E. Mast, P. Littrup, N. Duric, S. A. Johnson, and F. Wuebbling, "Comparison of ultrasound tomography methods in circular geometry," *Proc. SPIE*, vol. 4687, pp. 362–377, 2002.

[6] N. Duric, P. Littrup, L. Poulo, A. Babkin, R. Pevzner, E. Holsapple, O. Rama, and C. Glide, "Detection of breast cancer with ultrasound tomography: First results with the computerized ultrasound risk evaluation (C.U.R.E) prototype," *Med. Phys.*, vol. 34, no. 2, pp. 773–785, Feb. 2007.

[7] R. G. Pratt, L. Huang, N. Duric, and P. Littrup, "Sound-speed and attenuation imaging of breast tissue using waveform tomography of transmission ultrasound data," *Proc. SPIE*, vol. 6510, art. no. 65104S, 2007.

[8] K. W. A. van Dongen and W. M. D. Wright, "A full vectorial contrast source inversion scheme for three-dimensional acoustic imaging of both compressibility and density profiles," *J. Acoust. Soc. Am.*, vol. 121, no. 3, pp. 1538–1549, Mar. 2007.

[9] B. U. Karbeyaz, E. L. Miller, and R. O. Cleveland, "Shape-based ultrasound tomography using a Born model with application to high intensity focused ultrasound therapy," *J. Acoust. Soc. Am.*, vol. 123, no. 5, pp. 2944–2956, May. 2008.

[10] O. S. Haddadin, S. D. Lucas, and E. S. Ebbini, "Solution to the inverse scattering problem using a modified distorted born iterative algorithm," in *IEEE Ultrasonics Symp. Proc.*, 1995, pp. 1411–1414.

[11] P. R. Stepanishen, "The time-dependent force and radiation impedance on a piston in a rigid infinite planar baffle," *J. Acoust. Soc. Am.*, vol. 49, no. 3B, pp. 841–849, 1971.

[12] P. R. Stepanishen, "Transient radiation from pistons in an infinite planar baffle," *J. Acoust. Soc. Am.*, vol. 49, no. 5B, pp. 1627–1638, 1971.

[13] J. A. Ketterling, "Acoustic field of a wedge-shaped section of a spherical cap transducer," *J. Acoust. Soc. Am.*, vol. 114, no. 6, pt. 1, pp. 3065–3075, 2003.

[14] P. Wu and T. Stepinski, "Spatial impulse response method for predicting pulse-echo fields from a linear array with cylindrically concave surface," *IEEE Trans. Ultrason. Ferroelectr. Freq. Control*, vol. 46, no. 5, pp. 1283–1299, 1999.

[15] J. A. Jensen, "A new calculation procedure for spatial impulse responses in ultrasound," *J. Acoust. Soc. Am.*, vol. 105, no. 6, pp. 3266–3274, Oct. 1999.

[16] B. Piwakowski and K. Sbai, "A new approach to calculate the field radiated from arbitrarily structured transducer arrays," *IEEE Trans. Ultrason. Ferroelectr. Freq. Control*, vol. 46, no. 2, pp. 422–440, Mar. 1999.

[17] J. Goodman, *Introduction to Fourier Optics*, 3rd ed. Greenwood Village, CO: Roberts and Co., 2005.

[18] B. U. Karbeyaz, E. L. Miller, and R. O. Cleveland, "Semi-analytical computation of the acoustic field of a segment of a cylindrically concave transducer in lossless and attenuating media," *J. Acoust. Soc. Am.*, vol. 121, no. 2, pp. 1226–1237, Feb. 2007.

[19] P. R. Stepanishen and K. C. Benjamin, "Forward and backward projection of acoustic fields using FFT methods," *J. Acoust. Soc. Am.*, vol. 71, no. 4, pp. 803–812, Apr. 1982.

[20] P. Wu and T. Stepinski, "Extension of the angular spectrum approach to curved radiators," *J. Acoust. Soc. Am.*, vol. 105, no. 5, pp. 2618–2627, May. 1999.

[21] T. D. Mast, "Fresnel approximations for ultrasonic fields of rectangularly symmetric sources," *J. Acoust. Soc. Am.*, vol. 121, no. 6, pp. 3311–3322, 2007.

[22] T. D. Mast, L. Souriau, D.-L. Liu, M. Tabei, A. Nachmann, and R. Waag, "A k-space method for large-scale models of wave propagation in tissue," *IEEE Trans. Ultrason. Ferroelectr. Freq. Control*, vol. 48, no. 2, pp. 341–354, Mar. 2001.

[23] A. V. Oppenheim, R. W. Schafer, and J. R. Buck, *Discrete-Time Signal Processing*. 2nd ed. Upper Saddle River, NJ: Prentice-Hall, 1999.

[24] S. K. Mitra, *Digital Signal Processing*, 2nd ed. Boston, MA: McGraw Hill, 2002.

[25] G. Strang, *Introduction to Linear Algebra*, 2nd ed. Wellesley, MA: Wellesley-Cambridge Press, 1998.

[26] G. H. Golub and C. F. Van Loan, *Matrix Computations*, 3rd ed. Baltimore, MD: Johns Hopkins University Press, 1996.

[27] P. P. Vaidyanathan, *Multirate Systems and Filter Banks*. Upper Saddle River, NJ: Prentice Hall, 1993.

[28] A. D. Pierce, *Acoustics—An Introduction to Its Physical Principles and Applications*. Melville, NY: Acoustical Society of America, 1989.

[29] R. N. Bracewell, *The Fourier Transform and its Applications*. Boston, MA: McGraw Hill, 2000.

[30] S. W. Smith, *Scientist and Engineer's Guide to Digital Signal Processing*, 2nd ed. San Diego, CA: California Technical Publishing, 1999.

[31] D. E. Dudgeon and R. M. Mersereau, *Multidimensional Digital Signal Processing*. Upper Saddle River, NJ: Prentice Hall, 1983.

[32] W. C. Chew, *Waves and Fields in Inhomogeneous Media*. Piscataway, NJ: IEEE Press, 1999.

[33] X. Li and G. Qian, "Block size considerations for multidimensional convolution and correlation," *IEEE Trans. Signal Process.*, vol. 40, no. 5, pp. 1271–1273, May. 1992.

[34] M. Leutenegger, (2009, Feb.) "Error function of complex numbers," MATLAB program. [Online]. Available: http://www.mathworks.com/matlabcentral/fileexchange/18312

H. Emre Güven received the B.S. degree in 2003 and the M.S. degree in 2005, both in electrical and electronics engineering at Bilkent University, Ankara, Turkey. He is currently working towards the Ph.D. degree at Northeastern University. His research interests include signal and image processing, statistical estimation, and inverse problems. Mr. Guven is a member of Eta Kappa Nu and IEEE Signal Processing Society.

Eric L. Miller received the S.B. degree in 1990, the S.M. degree in 1992, and the Ph.D. degree in 1994, all in electrical engineering and computer science at the Massachusetts Institute of Technology, Cambridge, MA. He is currently a professor in the Department of Electrical and Computer Engineering at Tufts University and an Adjunct Professor of Computer Science, also at Tufts. Dr. Miller's research interests include physics-based tomographic image formation and object characterization, inverse problems in general and inverse scattering in particular, regularization, statistical signal and image processing, and computational physical modeling. This work has been carried out in the context of applications including medical imaging, nondestructive evaluation, environmental monitoring and remediation, landmine and unexploded ordnance remediation, and automatic target detection and classification.

Dr. Miller is a member of Tau Beta Pi, Phi Beta Kappa, and Eta Kappa Nu. He received the CAREER Award from the National Science Foundation in 1996 and the Outstanding Research Award from the College of Engineering at Northeastern University in 2002. He is currently serving as an Associate editor for the *IEEE Transactions on Geoscience and Remote Sensing* and was in the same position at the *IEEE Transactions on Image Processing* from 1998 to 2002. Dr. Miller was the co-general chair of the 2008 IEEE International Geoscience and Remote Sensing Symposium held in Boston, MA.

Robin O. Cleveland received his B.Sc. and M. Sc. degrees in physics from The University of Auckland (New Zealand) and a Ph.D. degree in mechanical engineering from the University of Texas at Austin. In 1995, he was awarded the F. V. Hunt post-doctoral fellowship of the Acoustical Society of America which was carried out at the University of Washington at Seattle. He joined the faculty of Boston University in 1997, where he is currently an Associate Professor of Mechanical Engineering. Dr. Cleveland's research interest is in the propagation of nonlinear sound in complex media and recent projects include: shock wave lithotripsy, therapeutic ultrasound, diagnostic ultrasound, and contrast agents. He is a Fellow of the Acoustical Society of America, an Associate Editor of the *Journal of the Acoustical Society of America*, a member of the Young Scientist Advisory Committee to the International Congress on Ultrasonics and faculty advisor to the Boston University Rocket Team.